



Microstructural and Mechanical Properties of One-Step Quenched and Partitioned 65Mn Steel

Muhammad Arslan Hafeez¹

Received: 22 August 2020 / Accepted: 23 October 2020 / Published online: 9 November 2020
© King Fahd University of Petroleum & Minerals 2020

Abstract

The novel quenching and partitioning processes concerned with the stabilization of carbon enriched austenite and provision of higher strength with higher toughness. The microstructural and mechanical properties of one-step quenched and partitioned 65Mn steel were investigated under various partitioning times, ranging from 30 to 600 s. The optical microscopy revealed that microstructure transformed from ferrite and pearlite to supersaturated lath martensite and retained austenite phases after one-step quenching and 30 s of partitioning. The unstable epsilon carbides were nucleated with the increase in partitioning time to 60 s and 180 s, whereas a further increase in partitioning time to 300 s transformed these unstable epsilon carbides into a stable cementite phase. Prolonged partitioning for 600 s produced carbon depleted martensite phase and nucleated ferrite phase. A maximum improvement of 88% in hardness and tensile strength and maximum reduction of 64% in elongation and 44% in impact toughness were achieved after 30 s of partitioning, compared to the as-received steel sample. On the other hand, partitioning for 600 s offered almost identical mechanical properties to the as-received steel. Partitioning for 180 s offered an optimum combination of mechanical properties of one-step quenched and partitioned 65Mn steel.

Keywords One-step quenching and partitioning · 65Mn steel · Carbon enriched austenite · Carbon depleted martensite · Mechanical properties

1 Introduction

The applications of advanced high strength (AHS) steels are increasing progressively in automotive and other applications because of their excellent amalgamation of properties. These properties include high strength, high ductility, reduced weight, excellent crash resistance, great energy absorption capacity, fatigue resistance, formability, weldability, efficient fuel consumption, reduced CO₂ emission, better environmental impact, and low costs [1–4]. Due to excellent amalgamation of properties, AHS steels are used in chassis, body-in-white (BIW) components, such as A-pillars, B-pillars, front cross member, side sills, roof railing, longitudinal beams, bumper reinforcements, door, hoods, and trunks in the automotive industry [5, 6]. A variety of AHS steels have been developed in the last decade and are classified into three

generations based on their mechanical properties [7, 8]. First-generation AHS steels, having ferrite-based microstructure, 500–1600 MPa tensile strength, and 5–30% elongation [9], include transformation induced plasticity (TRIP) steels, complex-phase steels, martensitic (MART) steels, and dual-phase (DP) steels [10–12]. Similarly, the second-generation AHS steels, having austenitic microstructure, comprise Al-added lightweight induced plasticity (L-IP) steels, twinning induced plasticity (TWIP) steels, and shear band strengthened (SIP) steels [13]. To further improve the mechanical properties of AHS steels, the third-generation of AHS steels, having an amalgamation of properties of first- and second-generations, was developed [14]. Third-generation AHSS steels comprise multiphase microstructure, including ferrite, retained austenite, bainite, and martensite similar to the first-generation steels [15], and offer improved fractions of retained austenite and improved UTS (500–1600 MPa) and elongation (25–50%) similar to the second-generation AHS steels at low cost [16]. Third-generation AHS steels include medium Mn steels, lightweight steels, advanced bainitic steels, quenched and partitioned (Q and P) steels, and quenched–partitioned–tempered (QPT) steels [17].

✉ Muhammad Arslan Hafeez
muhammad_arslanhafeez@yahoo.com

¹ School of Civil and Environmental Engineering, National University of Sciences and Technology, Islamabad 44000, Pakistan



The Q and P are a novel heat treatment process, proposed by J.G. Speer and co-workers in 2003 to develop a new AHS steel for automotive applications [18]. The Q and P heat treatment process is comprised of various stages, such as austenitizing above critical temperature, partial quenching between martensite start (M_s) and martensite finish (M_f) temperatures [19], and finally the partitioning treatment [20]. Partitioning treatment can be performed either at the same quenching temperature in a combined stage, called one-step Q and P process [21, 22] or above M_s temperature in a separate stage, called two-step Q and P process [23, 24]. Austenitizing completely transforms previous microstructure into the austenite phase, quenching between M_s and M_f partially transforms this austenite phase into a supersaturated martensite phase. Partitioning treatment causes carbon diffusion from the supersaturated martensite to retained austenite and stabilizes it to room temperature [25]. Finally, a duplex microstructure, having martensite and retained austenite is achieved. Martensite provides superior tensile strength, whereas retained austenite offers excellent impact toughness. Due to combined quenching and partitioning stages, one-step Q and P heat treatment process is more economical and easy to perform [21].

65Mn steel is a specified material widely used for rotary blades, having comprehensive mechanical properties [26]. For large tilling depth rotary tillage, the requirements of hard surface as well as tenacious core of the rotary blade still cannot be fulfilled [27]. Therefore, the improvement of mechanical properties of 65Mn steel is one of the urgent and important key matters, which needs immediate further work to fulfill the requirements of modern agricultural machinery manufacturing industries [28].

The current work aims to investigate the microstructural and mechanical properties of one-step Q and P heat-treated 65Mn steel. For this purpose, 65Mn steel was subjected to one-step Q and P heat treatment for various partitioning times, ranging from 30 to 600 s. The light optical microscope, micro Vickers hardness tester, tensile tester, and Charpy V-notch impact testers were utilized to evaluate the microstructure and mechanical properties of Q and P heat-treated 65Mn steel.

2 Experimental Work

2.1 Material

65Mn steel of chemical composition given in Table 1, selected for one-step Q and P heat treatment processes, was obtained in the form of a sheet of a thickness of 10 mm. Samples of required dimensions were machined by computer numerical control wire cut machine for subsequent heat treatment processes and characterization.

Table 1 Chemical composition of 65Mn steel (wt %)

C	Si	Mn	Cr	Ni	Cu	S	P	Fe
0.64	0.33	1.13	0.19	0.22	0.24	0.03	0.04	Bal.

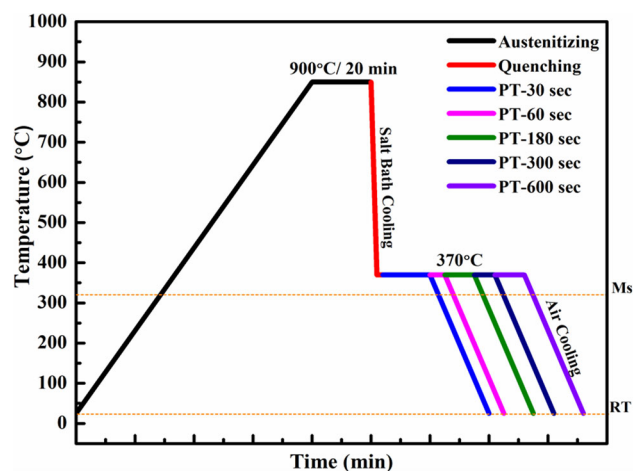


Fig. 1 Schematic of one-step Q and P heat-treatment processes, applied to 65Mn steel

2.2 One-Step Quenching and Partitioning Process

The one-step Q and P heat-treatment processes were started with austenitizing at 900 °C for 20 min, followed by controlled quenching at 370 °C temperature slightly above the martensite start temperature (M_s) in a salt bath furnace. The M_s temperature, calculated by the Nehernberg Eq. (1), was 325 °C [29]. Partitioning was also performed by isothermal holding at the same temperature of 370 °C for various partitioning times, i.e., 30, 60, 180, 300, and 600 s, followed by environment cooling too room temperature. The one-step Q and P heat-treatment processes, applied to 65Mn steel, are schematically presented in Fig. 1. The heat-treated samples were then washed and dried for subsequent characterization.

$$M_s = 498.9 - 300C - 33.3Mn - 22.2Cr - 16.7Ni - 11.1(Si + Mo) \quad (1)$$

2.3 Metallography

To evaluate the microstructure of one-step Q and P heat-treated 65Mn steel, samples of dimensions 10 mm³ were metallographically prepared by manual grinding on SiC papers of grades P100, P200, P400, P600, P800, and P1000 and polishing on velvet and nylon clothes with diamond pastes of grades grade 6, 3, 1 and 0.25 μm, using automatic grinder/polisher (Ecomet 250 Grinder Polisher, USA). Ground and polished samples were then etched in a 3 vol %

nital solution for 10 s. The microstructures of all samples were analyzed on a light optical microscope (Leica Model DM 15000 M, Germany) at 1000 × magnification.

2.4 Hardness Testing

Micro Vickers hardness testing was performed on micro Vickers hardness tester (Shimadzu Model HMV Japan) equipped with diamond indenter under the load of 1000 g for 10 s. Five readings were taken and averaged to get the final value for each sample.

2.5 Tensile Testing

For tensile testing, sample dimensions and testing procedure, mentioned in ASM E8/E8M standard, were adopted. Tensile testing was carried out on samples of gauge length 200 mm, width 40 mm, and radius of fillet 25 mm, using a tensile testing machine (Kelson's Brand, India), equipped with 400 KN load cell and extensometer at room temperature.

2.6 Impact Toughness Testing

Impact toughness values of all 65Mn steel samples were determined by performing Charpy V-notch impact test on samples of dimensions 10 mm × 10 mm × 55 mm with 2 mm V notch depth, using Charpy impact tester (Avery Denison, USA), equipped with 300 J hammer. Three tests were performed for each sample, and the final value was obtained by averaging the three values.

3 Results and Discussion

3.1 Microstructure Evolution

The austenitizing process dissolves all the previous phases into the austenite phase, partial quenching between M_S and M_f partially transforms this austenite into packets and blocks of lath martensite with retained austenite. At this stage, the stability and volume fractions of retained austenite are not enough to provide sufficient toughness. So, the partitioning process is performed at the same temperature to diffuse back C and N from martensite into austenite [1, 30, 31] as previously reported by Wang et al. [2] and Tariq et al. [32]. Optical micrographs of as-received and one-step Q and P heat-treated 65Mn steel are illustrated in Fig. 2. It was observed that the microstructure of 65Mn steel in as-received form comprised ferrite phase in two morphologies, including grain boundary allotriomorphic ferrite and idiomorphic ferrite, with lamellar pearlite (Fig. 2a). The microstructure of 65Mn steel was observed to be highly sensitive to isothermal partitioning times as evident by the formation of packets and blocks

of supersaturated lath martensite with minute fractions of retained austenite after 30 s of partitioning (Fig. 2b) similar to the work of Kong et al. [21]. The supersaturated lath martensite is considerably unstable not only due to the presence of excess carbon, but also due to greater intra crystal dislocation density and larger areas of bonding interfaces of the fine martensite crystals [33]. Wang et al. [34] also reported that austenitic partitioning behavior varied with volume fractions of austenite and resulted in nonhomogeneous segregation of carbon in austenite after the partitioning process.

Increasing of isothermal partitioning time leads to lattice relaxation of lath martensite by carbon diffusion from martensite into retained austenite and secondary phase carbides and enhanced the stability of both martensite and austenite, similar to the work of Wang et al. [34]. Therefore, a reduction in the volume fractions of martensite phase, improvement in the volume fraction of retained austenite phase, and nucleation of unstable transition carbides like epsilon carbide ($Fe_{2.4}C$) or eta carbide were observed in the microstructure of 65Mn steel, partitioned for 60 and 180 s, as illustrated in Fig. 2c and d. Further increasing of partitioning time to 300 s, unstable transition carbides transformed into stable carbide like cementite (Fe_3C) as previously reported by Speer et al. [35] presented in Fig. 2e. Prolonged isothermal partitioning for 600 s caused nucleation of ferrite with minor fractions of martensite and retained austenite Fig. 2f. The major phases present at this stage are retained austenite, ferrite, and supersaturated lath martensite. The ferrite phase is still referred to as carbon depleted martensite because it was nucleated from martensite and still has some morphological features of martensite.

3.2 Tensile Properties

Variations in tensile properties, such as tensile strength (R_m), yield strength ($R_{p0.2}$), elongation (ϵ_T), reduction in area (R_A), and yield ratio (YR), of as-received and one-step Q and P heat-treated 65Mn steel with varying isothermal partitioning time, are tabulated in Table 2. Considerable variations in tensile properties were observed with increasing partitioning time from 30 to 600 s. In as-received form, 65Mn steel exhibited the lowest values of R_m and $R_{p0.2}$ and the highest values of ϵ_T and R_A , which might be attributed to the presence of softer ferrite and pearlite in the microstructure. Strengthening of steels is possible by various mechanisms, such as grain boundaries strengthening, solid solution strengthening, point defect strengthening, martensitic strengthening, strain hardening, grain size reduction strengthening, and precipitation strengthening mechanisms [36–39]. The transformation of prior austenite into supersaturated lath martensite by diffusionless shear-type transformation mechanism is known as martensitic strengthening [40, 41]. In current work, 65Mn steel was strengthened by martensitic strengthening and pre-

Fig. 2 Optical micrographs of as-received and one-step Q and P heat-treated 65Mn steel under various partitioning times (a) as-received, (b) 30 s, (c) 60 s, (d) 180 s, (e) 300 s, and (f) 600 s

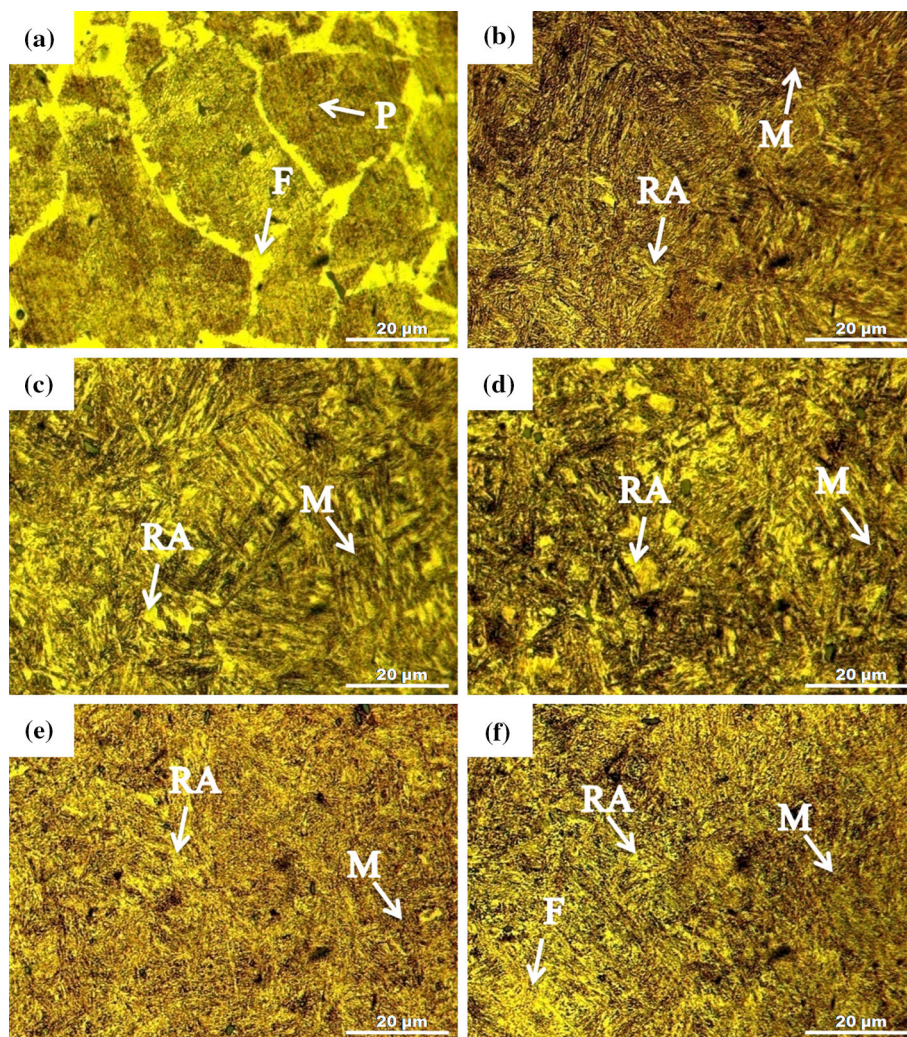


Table 2 Tensile properties of as-received and one-step Q and P heat-treated 65Mn steel

Sample ID	R_m (MPa)	$R_{P0.2}$ (MPa)	ϵ_T (%)	R_A (%)	YR	$R_m \times \epsilon_T$ (GPa. %)
AR	853	805	22	39	0.94	18.766
P-30	1597	1431	8	7.5	0.90	12.776
P-60	1478	1390	12	12	0.94	17.736
P-180	1409	1298	15	19	0.92	21.135
P-300	1234	1153	17	27	0.93	20.978
P-600	910	819	20	33	0.90	18.200

precipitation strengthening mechanisms after one-step Q and P heat treatment processes. The martensitic strengthening occurs due to two factors; first is higher dislocation density of martensite and the other is the formation of clusters of carbon with dislocations. Both factors hinder the motion of dislocations and ultimately strengthen the steel [42, 43].

Therefore, one-step Q and P heat treatment process performed for 30 s caused maximum 87% improvement in R_m , 78% improvement in $R_{P0.2}$, and maximum 64% reduction in ϵ_T and 81% reduction in R_A , compared to as-received steel,

which might be attributed to the microstructure comprised the highest volume fractions of lath martensite and minor volume fractions of retained austenite. Similarly, the partitioning for 60 s caused a 73% improvement in R_m and $R_{P0.2}$, and a 45% reduction in ϵ_T and a 69% reduction in R_A , compared to as-received steel. The partitioning for 60 s provided relatively less improved R_m and $R_{P0.2}$ and less reduced ϵ_T and R_A , compared to 30 s of partitioning due to diffusion of carbon from martensite into retained austenite during partitioning and an increase in volume fractions of retained austenite.



It has been reported that the austenite phase possesses a particular face-centered cubic lattice with four close-packed planes, each having three close-packed directions. Due to a large number of close-packed planes and directions, dislocations move very easily within the face-centered cubic austenite phase [44]. Further increase in partitioning time to 180 s and 300 s provided 65% and 45% improved R_m and 32% and 23% reduced ϵ_T , compared to as-received 65Mn steel, respectively. This is because of the phase transformation, including carbon diffusion from martensite to retained austenite, nucleation of unstable transition carbides, the formation of cementite, and minimization of supersaturation of martensite. Prolonged partitioning for 600 s provided tensile properties quite identical with as-received 65Mn steel attributed to the ferrite nucleation, which fully relieved the martensitic supersaturation.

3.3 Impact Toughness

Charpy V-notch impact test was performed at room temperature on as-received and one-step Q and P heat-treated 65Mn steel. The variations in impact toughness values as a function of partitioning times are plotted in Fig. 3. In as-received form 65Mn steel exhibited moderate impact toughness value (18 J), attributed to the presence of large volume fractions of pearlite and small fractions of ferrite in the microstructure. Application of quenching and partitioning for 30 s resulted in highly brittle steel exhibiting 44% reduced the lowest impact toughness value (10 J), compared to as-received steel. This is due to the formation of supersaturated lath martensite, which significantly improved the strengths but made the steel highly brittle. Partitioning for 60, 180, and 300 s gradually eliminated the brittleness and minimized the supersaturation of martensite by carbon diffusion from martensite to retained austenite and secondary phase transition carbides. Consequently, much better impact toughness values (14 J, 18 J, 22 J, respectively) were achieved compared with 30 s of partitioning. After prolonged partitioning for 600 s, steel became fully ductile even more than as-received steel. Nucleation of ferrite at this stage fully relieved the supersaturation of martensite and thus caused the highest 78% improved impact toughness value (32 J) compared to as-received steel.

3.4 Micro Vickers Hardness

In the one-step Q and P heat treatment process, partitioning time was observed to have a considerable impact on micro Vickers hardness of 65Mn steel. Variations in micro Vickers hardness values of 65Mn steel as a function of partitioning times are plotted in Fig. 4. 65Mn steel was observed to be very soft in as-received form as evidenced by very low hardness value of 233 VHN, attributed to the softer ferrite and pearlite in the microstructure. But, after the application of quench-

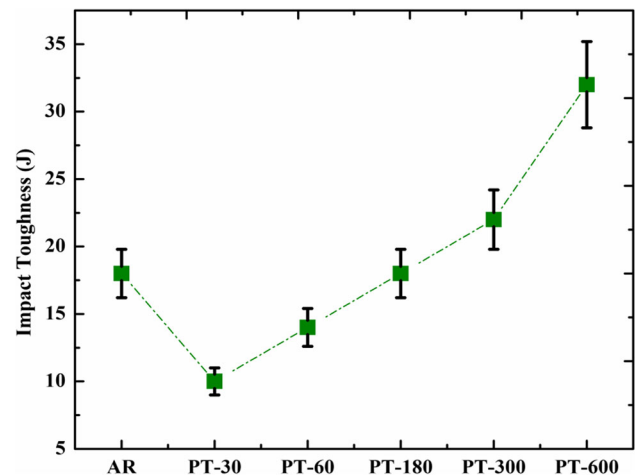


Fig. 3 Variations in impact toughness of as-received and one-step Q and P heat-treated 65Mn steel as function of partitioning time

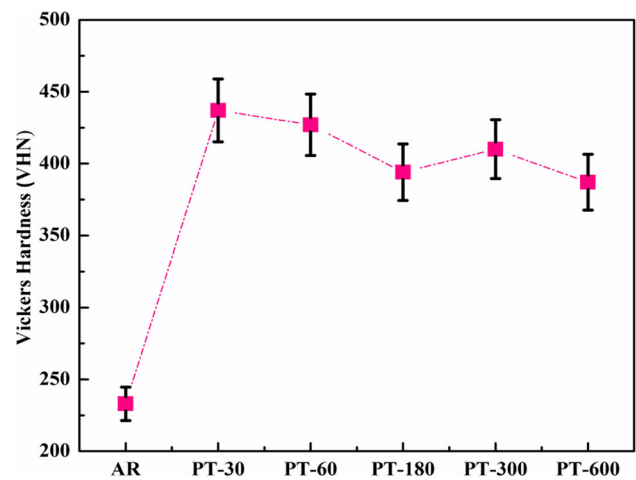


Fig. 4 Variations in micro Vickers hardness of as-received and one-step Q and P heat-treated 65Mn steel as function of partitioning time

ing and partitioning for 30 s, a drastic increase in 88% was observed in the Vickers hardness of 65Mn steel, which can be associated with the phase transformation from ferrite, pearlite into martensite and retained austenite. With the increasing of partitioning time to 60 s and 180 s, a reduction of 2% and 10% in Vickers hardness was observed, compared to samples partitioned for 30 s. This is because of the nucleation of the unstable carbides, which extracted the carbon from martensite and reduced the hardness value. A reduction in carbon concentration in martensite also caused a reduction in the tetragonality of martensite and thus resulted in a reduction in hardness similar to the work of Wendler et al. [5]. It has been reported that the carbon diffusion mechanism during partitioning for moderate time causes a reduction in micro Vickers hardness followed by a slight improvement [45, 46]. Therefore, after partitioning for 300 s, a slight increase in Vickers hardness (411 VHN) was observed, which can be

related to the transition of unstable carbides into the Fe_3C phase. Minimum improvement of 66% was demonstrated by the sample partitioned for 600 s, attributed to the nucleation of ferrite.

4 Conclusion

The effect of partitioning times on microstructural and mechanical properties of one-step Q and P heat-treated 65Mn steel was investigated. Following conclusions were extracted from this work;

1. Partitioning for 30 s produced microstructure, comprising packets and blocks of supersaturated lath martensite with retained austenite. Due to shorter time duration, minimum carbon diffusion occurred and thus resulted in maximum improvement of 88% in hardness and R_m and 78% in $R_{p0.2}$ and maximum reduction of 64% in \mathcal{E}_T , 81% in R_A , and 44% in impact toughness, compared to as-received steel sample.
2. Partitioning for 60–300 s caused further carbon diffusion from supersaturated martensite into retained austenite, nucleation of unstable transition carbides and formation of Fe_3C phase, resulted in 69–83% improvement in Vickers hardness, 45–73% in R_m , 43–73% in $R_{p0.2}$ with sufficient values of \mathcal{E}_T , R_A , and impact toughness.
3. Partitioning for 600 s, nucleated ferrite by further relieving supersaturated martensite, offered lowest values of hardness, strengths, and highest values of elongation and impact absorption energy among Q and P heat-treated samples. An optimum combination of R_m (1409 MPa), \mathcal{E}_T (15%) impact toughness (18 J), and Vickers hardness (394 HV) was achieved after partitioning for 180 °C.

References

1. Forouzan, F.; Vuorinen, E.; Mücklich, F.: Post weld-treatment of laser welded AHSS by application of quenching and partitioning technique. *Mater. Sci. Eng., A* **698**, 174–182 (2017)
2. Wang, M.M.; Hell, J.C.; Tasan, C.C.: Martensite size effects on damage in quenching and partitioning steels. *Scr. Mater.* **138**, 1–5 (2017)
3. Allain, S.Y.P.; Geandier, G.; Hell, J.C.; Soler, M.; Danoix, F.; Gouné, M.: In-situ investigation of quenching and partitioning by high energy X-ray diffraction experiments. *Scr. Mater.* **131**, 15–18 (2017)
4. Zou, D.Q.; Lia, S.H.; He, J.: Temperature and strain rate dependent deformation induced martensitic transformation and flow behavior of quenching and partitioning steels. *Mater. Sci. Eng., A* **680**, 54–63 (2017)
5. Chena, X.; Niu, C.; Lian, C.; Lin, J.: The evaluation of formability of the 3rd generation advanced high strength steels QP980 based on digital image correlation method. *Procedia Eng.* **207**, 556–561 (2017)
6. Mohammed, B.; Park, T.; Pourboghrat, F.; Hu, J.; Esmailpour, R.; Farha, F.A.: Multiscale crystal plasticity modeling of multiphase advanced high strength steel. *Int. J. Solids Struct.* **151**, 57–75 (2018)
7. Mohammed, B.; Park, T.; Kim, H.; Pourboghrat, F.; Esmailpour, R.: The forming limit curve for multiphase advanced high strength steels based on crystal plasticity finite element modeling. *Mater. Sci. Eng., A* **725**, 250–266 (2018)
8. Knijf, D.D.; Föjer, C.; Kestens, L.A.I.; Petrov, R.: Factors influencing the austenite stability during tensile testing of quenching and partitioning steel determined via in situ electron backscatter diffraction. *Mater. Sci. Eng., A* **638**, 219–227 (2015)
9. Paykani, M.A.; Shahverdi, H.R.; Miresmaeili, R.: First and third generations of advanced high-strength steels in a FeCrNiBSi system. *J. Mater. Process. Technol.* **238**, 383–394 (2016)
10. Liu, Qinglong; Zhou, Qingjun; Venezuela, Jeffrey; Zhang, M.; Atrens, A.: Hydrogen influence on some advanced high-strength steels. *Corros. Sci.* **125**, 114–138 (2017)
11. Kalhor, A.; Soleimani, M.; Mirzadeh, H.; Uthaisangasuk, V.: A review of recent progress in mechanical and corrosion properties of dual phase steels. *Arch. Civ. Mech. Eng.* **20**, 85 (2020)
12. Soleimani, M.; Kalhor, A.; Mirzadeh, H.: Transformation-induced plasticity (TRIP) in advanced steels: a review. *Mater. Sci. Eng., A* **795**, 140023 (2020)
13. Bhargava, M.; Tewari, A.; Mishra, S.K.: Forming limit diagram of advanced high strength steels (AHSS) based on strain-path diagram. *Mater. Des.* **85**, 149–155 (2015)
14. Pourmajidian, M.; McDermid, J.R.: On the reactive wetting of a medium-Mn advanced high-strength steel during continuous galvanizing. *Surf. Coat. Technol.* **357**, 418–426 (2019)
15. Park, T.; Hector, L.G.; Hu, J.X.; Farha, F.A.; Fellingner, M.R.; Kim, H.; Esmailpour, R.; Pourboghrat, F.: Crystal plasticity modeling of 3rd generation multi-phase AHSS with martensitic transformation. *Int. J. Plast* **120**, 1–46 (2019)
16. Sun, W.W.; Wu, Y.X.; Yang, S.C.; Hutchinson, C.R.: Advanced high strength steel (AHSS) development through chemical patterning of austenite. *Scr. Mater.* **146**, 60–63 (2018)
17. Srivastav, A.; Armaki, H.G.; Sung, H.; Chen, P.; Kumar, S.; Bower, A.F.: Micromechanics of plastic deformation and phase transformation in a three-phase TRIP-assisted advanced high strength steel: experiments and modeling. *J. Mech. Phys. Solids* **78**, 46–69 (2015)
18. Wang, Z.; Wang, K.; Liu, Y.; Zhu, B.; Zhang, Y.; Li, S.: Multi-scale simulation for hot stamping quenching and partitioning process of high-strength steel. *J. Mater. Process. Technol.* **269**, 150–162 (2019)
19. Nyssonen, T.; Peur, P.; Moor, E.D.; Williamson, D.; Kuokkal, V.T.: Crystallography and mechanical properties of intercritically annealed quench and partitioned high-aluminum steel. *Mater. Charact.* **148**, 71–80 (2019)
20. Casero, C.C.; Kwakernaak, C.; Sietsma, J.: The influence of the austenite grain size on the microstructural development during quenching and partitioning processing of a low-carbon steel. *Mater. Des.* **178**, 107847 (2019). <https://doi.org/10.1016/j.matdes.2019.107847>
21. Kong, H.; Chao, Q.; Rolfe, B.; Beladi, H.: One-step quenching and partitioning treatment of a tailor welded blank of boron and TRIP steels for automotive applications. *Mater. Des.* **174**, 107799 (2019)
22. Kong, H.; Chao, Q.; Cai, M.H.; Pavlina, E.J.; Rolfe, B.; Hodgson, P.D.; Beladi, H.: One-step quenching and partitioning treatment of a commercial low silicon boron steel. *Mater. Sci. Eng., A* **707**, 538–547 (2017)
23. Ebner, S.; Suppan, C.; Stark, A.; Schnitzer, R.; Hofer, C.: Austenite decomposition and carbon partitioning during quenching and partitioning heat treatments studied via in situ X-ray diffraction. *Mater. Des.* **178**, 107862 (2019)
24. Peng, F.; Xu, Y.; Li, J.: Interaction of martensite and bainite transformations and its dependence on quenching temperature in



- intercritical quenching and partitioning steels. *Mater. Des.* **181**, 107921 (2019)
25. Xia, P.; Vercruyssen, F.; Petrov, R.; Sabirov, I.; Rodríguez, M.C.; Verleysen, P.: High strain rate tensile behavior of a quenching and partitioning (Q&P) Fe–0.25C–1.5Si–3.0Mn steel. *Mater. Sci. Eng., A* **745**, 53–62 (2019)
 26. Wang, H.; Zhao, Y.; Yuan, X.; Chen, K.; Xu, R.: Effects of boronizing treatment on corrosion resistance of 65mn steel in two acid mediums. *Phys. Procedia* **50**, 124–130 (2013)
 27. Wang, Y.; Sun, J.; Jiang, T.; Yang, C.; Tan, Q.; Guo, S.; Liu, Y.: Super strength of 65Mn spring steel obtained by appropriate quenching and tempering in an ultrafine grain condition. *Mater. Sci. Eng., A* **754**, 1–8 (2019)
 28. Chunjie, D.; Jianhua, Z.; Jiayuan, X.; Xichao, S.; Yunfeng, Z.: Microstructures and properties of electrical discharge strengthened layers on 65Mn steel. *Appl. Surf. Sci.* **257**, 2843–2849 (2011)
 29. Liu, C.; Zhao, Z.; Northwood, D.O.; Liu, Y.: A new empirical formula for the calculation of MS in pure iron super low alloy steels. *J. Mater. Process. Technol.* **113**, 556–562 (2001)
 30. Wendler, M.; Ullrich, C.; Hauser, M.; Krüger, L.; Volkova, O.; Wei, A.; Mola, J.: Quenching and partitioning (Q and P) processing of fully austenitic stainless steels. *Acta Mater.* **133**, 346–355 (2017)
 31. Santofimia, M.J.; Petrov, R.H.; Zhao, L.; Sietsma, J.: Microstructural analysis of martensite constituents in quenching and partitioning steels. *Mater. Charact.* **92**, 91–95 (2014)
 32. Tariq, F.; Baloch, R.A.: One-step quenching and partitioning heat treatment of medium carbon low alloy steel. *J. Mater. Eng. Perform.* **23**, 1726–1739 (2014)
 33. Elena P.; David V. Edmonds, Phase transformation in steels. *woodhead* 138 (2012)
 34. Wang, C.Y.; Shi, J.; Cao, W.Q.; Dong, H.: Characterization of microstructure obtained by quenching and partitioning process in low alloy martensitic steel. *Mater. Sci. Eng., A* **527**, 3442–3449 (2010)
 35. Speer, J.G.: Phase transformation in quenched and partitioned steel. *Phase Transf. Steel* **2**, 247–268 (2012)
 36. Goerge E. Dieter, strengthening mechanisms in mechanical metallurgy book, 3rd edition 184–233 (2017)
 37. Callister, W.D.; David, J.; Rethwisch, G.: Dislocation and strengthening mechanisms in material science and engineering an introduction book, 8th edition 188–191 (2009)
 38. Hafeez, M.A.; Farooq, A.; Tayyab, K.B.; Arshad, M.A.: Effect of thermo-mechanical cyclic quenching and tempering treatments on microstructure, mechanical, and electrochemical properties of AISI 1345 steel. *Int. J. Miner. Metall. Mater.* (2020). <https://doi.org/10.1007/s12613-020-2139-4>
 39. Hafeez, M.A.; Usman, M.; Arshad, M.A.; Umer, M.A.: Nanoindentation-based micro-mechanical and electrochemical properties of quench-hardened, tempered low-carbon steel. *Crystals* **10**, 508 (2020)
 40. Hafeez, M.A.: Investigation on mechanical properties and immersion corrosion performance of 0.35%C–10.5%Mn steel processed by austenite reverted transformation (ART) annealing process. *Metallogr. Microstruct. Anal.* **9**, 159–168 (2020)
 41. Hafeez, M.A.; Farooq, A.: Effect of heat treatments on the mechanical and electrochemical behavior of 38CrSi and AISI 4140 steels. *Metallogr. Microstruct. Anal.* **8**, 479–487 (2019)
 42. Hafeez, M.A.; Farooq, A.: Microstructural, mechanical and tribological investigation of 30CrMnSiNi2A ultra-high strength steel under various tempering temperatures. *Mater. Res. Express* **5**, 016505 (2018)
 43. Hafeez, M.A.: Effect of microstructural transformation during tempering on mechanical properties of quenched and tempered 38CrSi steel. *Mater. Res. Express* **6**, 086552 (2019)
 44. Abbaschian, R.; Abbaschian, L.; Reed-Hill, R.E.: *Physical Metallurgy Principles*, 4th edn, pp. 1–10. Cengage Learning, Stamford (2009)
 45. Nishikawa, A.S.; Santofimia, M.J.; Sietsma, J.; Goldensein, H.: Influence of bainite reaction on the kinetics of carbon redistribution during the quenching and partitioning (Q & P) processing of medium Mn steel. *Acta Mater.* **107**, 354–365 (2016)
 46. Clarke, A.J.; Speer, J.G.; Matlock, D.K.; Rizzo, F.C.; Edmond, D.V.; Santofimia, M.J.: Influence of carbon partitioning kinetics on final austenite fraction during quenching and partitioning. *Scr. Mater.* **61**, 149–152 (2009)

